



OPEN Long non-coding RNA PCAT18 defines a leukemia-specific regulatory network in pediatric T-ALL

F. Altieri¹✉, G. Pecoraro¹, V. Costabile¹, R. Penta de Vera d'Aragona², G. Becchimanzi³, G. Beneduce⁴, R. Parasole⁴ & G. Smaldone¹

Long non-coding RNAs (lncRNAs) have emerged as pivotal regulators of gene expression across various levels, including transcriptional, post-transcriptional, and epigenetic mechanisms. In pediatric T-cell acute lymphoblastic leukemia (T-ALL), dysregulated lncRNA expression contributes to altered cell proliferation, apoptosis resistance, treatment response, and disease progression. Our previous work identified a distinct lncRNA signature capable of differentiating T-ALL from B-ALL, highlighting their diagnostic potential. In our work, we focused on the lncRNA called PCAT18. We used RNA-seq analysis on 13 patients with T-ALL in comparison to cord blood cells. We performed a preliminary *in silico* analysis through WGCNA to reveal interesting co-expression network of target lncRNA. PCAT18 silencing in two T-ALL cell models allowed to investigate its functional role in physiological and pathological states. Finally, RNA-seq analyses of PCAT18 silenced cell line in comparison with control cell line was carried out to identify and confirm pathways significantly altered by its absence. Our network analysis (WGCNA) revealed that PCAT18 is highly connected within a module strongly associated with the T-ALL phenotype. Functional assays in JURKAT cells demonstrated that PCAT18 knockdown paradoxically enhanced proliferation, induced G1 phase accumulation, reduced p27 expression, and upregulated Cyclin B, suggesting disrupted checkpoint control and uncoordinated cell cycle progression. Additionally, deregulation of FOXP3, NOTCH3, HSP90AA1, and HSPA8 implicated PCAT18 in stress response pathways and lineage identity maintenance. These findings support a tumor-suppressive role for PCAT18 in T-ALL, in contrast to its oncogenic role in solid tumors. PCAT18 appears to operate at the intersection of transcriptional regulation, cell cycle control, and stress adaptation. Its disease- and lineage-specific expression makes it a promising candidate for biomarker development and therapeutic targeting in pediatric T-ALL. This study expands our understanding of lncRNA biology in leukemia and uncovers novel regulatory mechanisms in T-ALL pathogenesis.

T-cell acute lymphoblastic leukemia (T-ALL) is an aggressive haematological cancer originating from T-cell precursors that transformed from the thymus. Although T-ALL represents a minority of childhood ALL cases when compared with its B-cell counterpart, it is associated with a higher presenting leukocyte count, greater central nervous system involvement, and a particularly difficult clinical course^{1,2}. Although improvements in multi-agent chemotherapy and risk stratification are made, relapse and chemotherapy resistance remain significant challenges, particularly with the high risk or early-thymic precursor subtypes³. These limitations highlight the importance of finding new molecular players as potential biomarkers or targets for therapy.

In the past several years, studies on the pathogenesis of hematological malignancies have grown over and above a focus on protein-coding genes to encompass long non-coding RNAs (lncRNAs), a class of transcripts longer than 200 nucleotides conspicuously devoid of protein-coding potential, yet serving as regulators of diverse cellular activities⁴. lncRNAs play a central role in modulating gene expression via transcriptional, epigenetic and posttranscriptional means. These genes participate in a variety of biological actions, such as cell proliferation, apoptosis, cell cycle regulation, etc., and are typically characterized with high tissue and disease specificity^{5,6}.

¹IRCCS SYNLAB SDN, Via G. Ferraris 144, Naples, Italy. ²BASCO Unit, Cellular Manipulation and Immunogenetics, AORN Santobono-Pausilipon, AORN Santobono-Pausilipon, Naples 80122, Italy. ³Clinical Trial Center, Clinical and Translational Research Unit, AORN Santobono-Pausilipon, Naples 80122, Italy. ⁴Department of Oncology, Hematology and cellular therapy, Santobono-Pausilipon Children's Hospital, AORN, Naples 80122, Italy. ✉email: filomena.altieri@synlab.it

Significantly, lncRNAs are emerging not only as functional actors in tumour biology but also as potential diagnostic and prognostic biomarkers. Due to their cancer type-specific expression profiles, extreme stability in body fluids and their functional association with ontogenetic pathways, they appear to be promising for translational studies⁷. In acute lymphoblastic leukemia, the functional roles of lncRNAs are poorly defined. Nevertheless, our recent work has started to identify individual transcripts involved in B-ALL pathogenesis^{8,9}.

Turning our attention to T-ALL, in a recent study¹⁰ we identified a distinct lncRNA expression profile in paediatric cases, within which PCAT18 (Prostate Cancer Associated Transcript 18) emerged as a novel transcript associated with the disease. While this lncRNA has previously been linked to solid tumours, such as prostate and gastric cancers^{11,12}.

To date, PCAT18 has already been studied in haematological malignancies, but only in myeloid leukemia¹³, never in lymphoid leukemia. In this study, we aimed to explore the expression and biological function of PCAT18 in paediatric T-ALL, combining patient data, cell-based assays, and transcriptomic profiling, in order to assess its potential as a lineage-specific biomarker and regulatory player in T-cell leukemogenesis.

Methods

Study population

For this study, we enrolled 13 T-ALL paediatric patients. All participants provided informed assent through informed consent signed by both parents. A specific protocol, according with the Helsinki declaration, was accepted by the IRCCS Pascale Ethical Committee, (Naples- Italy, protocol number 5/19 of the 19 June 2019) and 1/23 (dated 8 February 2023) as well as the AORN Santobono-Pausilipon Cardarelli/Pausilipon Ethical Committee (Naples, Italy, protocol number 07/20 of 3 June 2020). Clinical information of enrolled patients was reported in Table 1.

Patient samples and cell lines

Bone Marrow Mononuclear Cells (BM-MNCs) of patients and Cord Blood Mononuclear Cells used as healthy controls were obtained from IRCCS SYNLAB SDN biobank¹⁴. Authenticated human leukemia T cell lines JURKAT and RPMI8402 were grown in RPMI-1640 medium, supplemented with heat inactivated FBS, 100 U/ml penicillin, 10 mg/mL streptomycin, 1% l-glutamine at 37 °C in a 5% CO₂ atmosphere.

Data preprocessing

Raw sequencing reads, retrieved from NCBI bioproject number PRJNA1263624, were preprocessed using fastp (v0.23.2)¹⁵ to remove adapter sequences, trim low-quality bases, and filter out reads with overall low quality. High-quality reads that passed filtering were subsequently aligned to the human reference genome (GRCh38.

	T ALL
Number (%)	13
Median Age at diagnosis (range)	7.5 years (range 1 -14 years)
Sex (%)	7 (53,8) Female 6 (46,2) Male
Race (%)	11 (84,6) caucasian 2(15,4) non caucasian
Hyperleukocytosis at diagnosis (%)	9 (69,2) > 100,000 ul 4 (30,7) < 100,000 ul
Cytogenetics (%)	8 (46,1) not available 1 (7,7) hyperdiploid 1 (7,7) 47,XX, + mar[5]/46,XX[5] 1 (7,7) 46, XX del 6q[9]/46, XX [6] 1 (7,7) 46,XY,-11, + mar[10]/46,XY[5] 1 (7,7) 47 XY, t(7;19)(q34;p13), + 8
Molecular biology (%)	10 (76,9) negative 3 (23,1) del 1
EGIL classification (%)	1 (7,7) EGIL T I/II 10 (76,7) EGIL T-III 1 (7,7) EGIL T- IV 1 (7,7) not available
Extramedullary status	3 (15) SNC 1 (7,7) skin 6 (46,1) mediastinum bulky 3 (23) no extramedullary disease
Risk	2 (15,6) non High risk 11 (84,4) High risk
Relapse	3 (23,1) relapse 10(76,9) no relapse
Alive	2 (15,8) death 10 (76,9) alive 1 (7,7) lost follow up

Table 1. Clinical information of enrolled patients.

p14) using the STAR aligner (v2.7.10a)¹⁶, employing the GENCODE Release 48 GTF annotation for accurate transcript mapping.

Post-alignment, SAM/BAM files were processed with SAMtools (v1.17)¹⁷ to sort reads by genomic coordinates. Quality control metrics at each step were assessed to ensure consistency across samples.

Gene-level quantification was performed using FeatureCounts (subread v2.0.3)^{18,19}, excluding multimapping and overlapping reads to ensure accurate gene count estimation. Individual gene count files were merged using a custom Python script into a single gene count matrix. Corresponding sample metadata, including condition (leukemia vs control), were stored in a separate metadata table for downstream statistical analysis.

To filter out lowly expressed genes, only those with a raw count ≥ 10 in at least 5 samples were retained. Data variance was stabilized using the variance-stabilizing transformation (VST) function from the DESeq2 package (v1.40.1)²⁰. Normalization of gene counts was carried out using DESeq2's internal normalization method to correct for sequencing depth and RNA composition biases.

Differential expression analysis

Differential gene expression analysis was performed using DESeq2. Genes with a $\log_2\text{FoldChange} \geq 2$ and an adjusted p-value < 0.05 (Benjamini–Hochberg correction) were considered significantly differentially expressed. This threshold was chosen to identify robust changes in gene expression between leukemia and control samples.

Co-expression network analysis

To investigate gene co-regulation patterns, we performed Weighted Gene Correlation Network Analysis (WGCNA)²¹ using the top 2,500 most variable genes across all samples. An unsigned adjacency matrix was constructed using a soft-thresholding power of 12, selected based on the scale-free topology criterion across multiple power settings. From the adjacency matrix, a Topological Overlap Matrix (TOM) was calculated to measure pairwise gene connectivity and minimize spurious correlations.

Genes were grouped into co-expression modules using dynamic tree cutting on the TOM-based dissimilarity matrix. Module eigengenes were then correlated with sample phenotypes to identify modules associated with disease status.

For visualization, the TOM matrix was used to generate network files (nodes and edges), which were exported for visualization in Cytoscape (v3.10.0)²². Each gene node was annotated with the $\log_2\text{FoldChange}$ and adjusted p-value from the DESeq2 differential expression results to highlight subnetworks significantly altered in leukemia samples.

mRNA isolation and qRT-PCR

Total RNA was extracted from Bone Marrow and Cord Blood Mononuclear Cells (BM-MNCs) of using TRIzol reagent solution (Thermo Fischer Scientific, Waltham, MA, USA) according to the manufacturer's protocol. cDNA was synthesized using the SuperScript III First-Strand Synthesis SuperMix kit (Thermo Fisher Scientific) according to the manufacturer's protocol. qRT-PCR was performed with the iQ SYBR Green Supermix (#1,708,882, Bio-Rad), each reaction was performed in triplicate. We used the $2^{-\Delta\Delta\text{CT}}$ method to calculate the relative expression levels and normalized against the reference ribosomal protein S18 gene (RPS18). Primers used for gene expression analysis are listed in Table 2.

Functional studies

Functional studies were performed on JURKAT cell line, which was treated with DsiRNAs against PCAT18 for 48 h. DNA-Prep Reagent Kit (607,055, Beckman Coulter, Brea, CA, USA) was used to analyse the cell cycle of scrambled and knocked-down JURKAT cells, with a minimum of 10,000 single-cell events recorded. The percentage of cells in G1, S and G2/M phases was calculated using the Dean–Jett–Fox model (DJF model). Cell cycle analysis was conducted using Kaluza Analysis Software version number 2.1 (<https://www.beckman.it/flow-cytometry/software/kaluza>, Beckman Coulter). Cell viability was detected using ATP Lite™ kit (6016943, PerkinElmer, Waltham, MA, USA) and ATP signal was measured using a Victor Nivo plate reader (PerkinElmer, Waltham, MA, USA). Cell cycle and ATP Lite analyses were conducted in triplicate with similar results.

Gene name	Primer forward	Primer reverse
RPS18	5'-CGATGGGCGGCGGAAAATA-3'	5'-CTGCTTTCCTCAACACCACA-3'
PCAT18	5'-GTCCAGCACTTCACTGGTT-3'	5'-AGCTGGGATATGGTAGCAGC-3'
CyclinA	5'-AAATGGGCGAGTACAGGAGGA-3'	5'-CCACAGTCAGGGAGTGCTTT-3'
CyclinB	5'-CATGGTGCACCTTTCCTCCTT-3'	5'-AGGTAATGTTGTAGAGTTGGTGTCC-3'
CyclinE	5'-GGCCAAAATCGACAGGAC-3'	5'-GGGTCTGCACAGACTGCAT-3'
CyclinD	5'-GCTGTGCATCTACACCGACA-3'	5'-TTGAGCTTGTTACACAGGAG-3'
HSP90AA1	5'-TCTGCCTCTGGTGATGAGATGG-3'	5'-CGTTCACAAAGGCTGAGTTAGC-3'
HSPA8 (HSC70)	5'-TCCTACCAAGCAGACACAGACC-3'	5'-CAGGAGGTATGCCTGTGAGTTC-3'
FOXP3	5'-GGCACAATGTCTCCTCCAGAGA-3'	5'-CAGATGAAGCCTTGGTCAGTGC-3'
NOTCH3	5'-ATGCAGGATAGCAAGGAGGA-3'	5'-AAGTGGTCCAACAGCAGCTT-3'

Table 2. Primers sequences user for qRT-PCR.

T-ALL blasts sorting

Fluorescence Activated Cell Sorting (FACS) was performed using the BD FACSMelody™ Cell Sorter (BD Biosciences, USA). PBMCs derived from the three bone marrow samples were resuspended in 200 µL of RPMI-1640 complete medium, followed by incubation with the following antibodies: BD Horizon™ RB545 Mouse Anti-Human CD4 (cat: 569,183, BD Biosciences) and BD Pharmingen™ APC Mouse Anti-Human CD8 (cat: 566,852, BD Biosciences) at 1:20 dilution. After incubation for 20' at RT in the dark, marked PBMCs were washed once with PBS 1× and resuspended in 2 mL of fresh 1% FBS 2 mM EDTA PBS 1x. Sorting was performed using the two-way sorter configuration and two sub-population were separated: CD4+/CD8- and CD4-/CD8+. Sorting efficiency was always kept above 95% and the collected cell populations were subsequently pelleted and resuspended in Trizol for further analysis.

RNA-seq from JURKAT cell line

Total RNA was extracted from PCAT18 knocked-down and control JURKAT cells in biological triplicates. Concentration and quality were assessed using Qubit (ThermoFisher Scientific, MA, USA) spectrophotometer. Total RNA-seq libraries were prepared for polyA selection of mRNA and sequenced in paired-end mode with Illumina Novaseq6000. The reference track was the Human assembly obtained from GenCode (Release 48, GRCh38.p14)³. The quantification of transcripts expressed for each sequenced samples was performed using featureCount algorithm⁵.

Statistical analyses

Statistical analyses were performed using GraphPad Prism Version 9. Mann–Whitney was used to assess the statistical significance of comparisons. P-values < 0.05 were considered statistically significant (< 0.05 = *; < 0.01 = **; < 0.001 = ***). For the functional experiments, error bars represent mean ± SD of, at minimum, three independent experiments.

Results

PCAT18 network analysis

Differential gene expression analysis was performed using DESeq2 on 13 T-cell acute lymphoblastic leukemia (T-ALL) samples and 15 cord blood mononuclear cell (CBMC) controls. The initial gene count matrix included 77,263 genomic elements derived from the comprehensive GENCODE Human GTF (GRCh38.p14). Low-count filtering reduced this set to 39,755 genes, which were then normalized and variance-stabilized using DESeq2's internal methods. Principal component analysis (PCA) on the log-transformed data revealed a clear separation between T-ALL and control samples (Supplementary Fig. 1).

Differential expression analysis identified 8,350 differentially expressed genes (DEGs) (adjusted $p < 0.05$, $|\log_2\text{FoldChange}| \geq 2$), comprising 3,887 upregulated and 4,463 downregulated genes in T-ALL relative to controls (Supplementary Table 1). A heatmap constructed from the 50 top variably expressed genes illustrates the distinct expression patterns across the two phenotypes (Fig. 1 and Supplementary Table 2).

WGCNA was conducted on the top 2,500 most variable genes (after low-count filtering consistent with the DEG analysis). The pickSoftThreshold function determined a soft-thresholding power (β) of 12 for constructing an unsigned network. Two major gene co-expression modules were identified using dynamic tree cutting with a permissive minimum module size of 200 genes (Fig. 2A). These modules showed strong associations with disease phenotype: the blue module was positively correlated with healthy controls ($r = 0.88$, Spearman), whereas the turquoise module correlated with the T-ALL phenotype ($r = 0.96$) (Fig. 2B–C).

A subnetwork centered on PCAT18 was extracted, comprising 61 neighboring genes. Nodes in the resulting network visualization (Fig. 3A and Supplementary Table 3) were color-coded based on $\log_2\text{FoldChange}$ values and shaped to indicate coding status (triangles for non-coding elements). To identify highly influential genes within the PCAT18 network, $\log_2\text{FoldChange}$ values were plotted against node degree (number of connections), highlighting key hub genes (Fig. 3B).

PCAT18 is upregulated in T-ALL patients and its silencing promotes cell proliferation and impairs cell cycle

Following our previous work, which identified PCAT18 as a core component of a lncRNA signature specifically linked to paediatric T-ALL¹⁰, we sought to better define its expression pattern in the disease. Flow cytometry cell sorting experiments revealed that PCAT18 expression was restricted to the blast population and undetectable in healthy T cells (Fig. 4A), reinforcing its disease-specific association. In light of these results, we next investigated the functional role of PCAT18 in T-ALL, JURKAT cell line, an immortalized T lymphocyte cell line chosen as an *in vitro* model was electroporated with PCAT18 specific siRNA and assessed the biological consequences at 48 h post-electroporation (Fig. 4B). First of all, we evaluated the effects of silencing on cell proliferation using a luminescent cell viability assay. Data obtained showed a significant increase in proliferation in PCAT18 knock out cells (JURKAT^{PCAT18-}) compared to controls (JURKAT^{ctrl}) (Fig. 4C). To further clarify the functional implications of PCAT18 on proliferation, we performed cell cycle analysis, which revealed a significant accumulation of cells in G1 phase and a decreased population of G2/M cells, suggesting that loss of PCAT18 led to a partial G1 arrest or dysregulated G1 and G2/M checkpoints (Fig. 4D). Having ascertained cell cycle dysregulation and knowing the importance of cyclin-dependent kinase (CDK) inhibitors in cell cycle progression, we decided to investigate the expression of CDK inhibitors alongside Cyclins. At the molecular level, we found that the cyclin-dependent kinase inhibitor p27 was significantly downregulated in JURKAT^{PCAT18-} cells respect to the JURKAT^{ctrl} cells (Fig. 4E). Interestingly, a similar relationship between p27 and PCAT18 has already been reported in gastric cancer²³ which suggests there might be a common mechanism at play here as well. However, gene expression

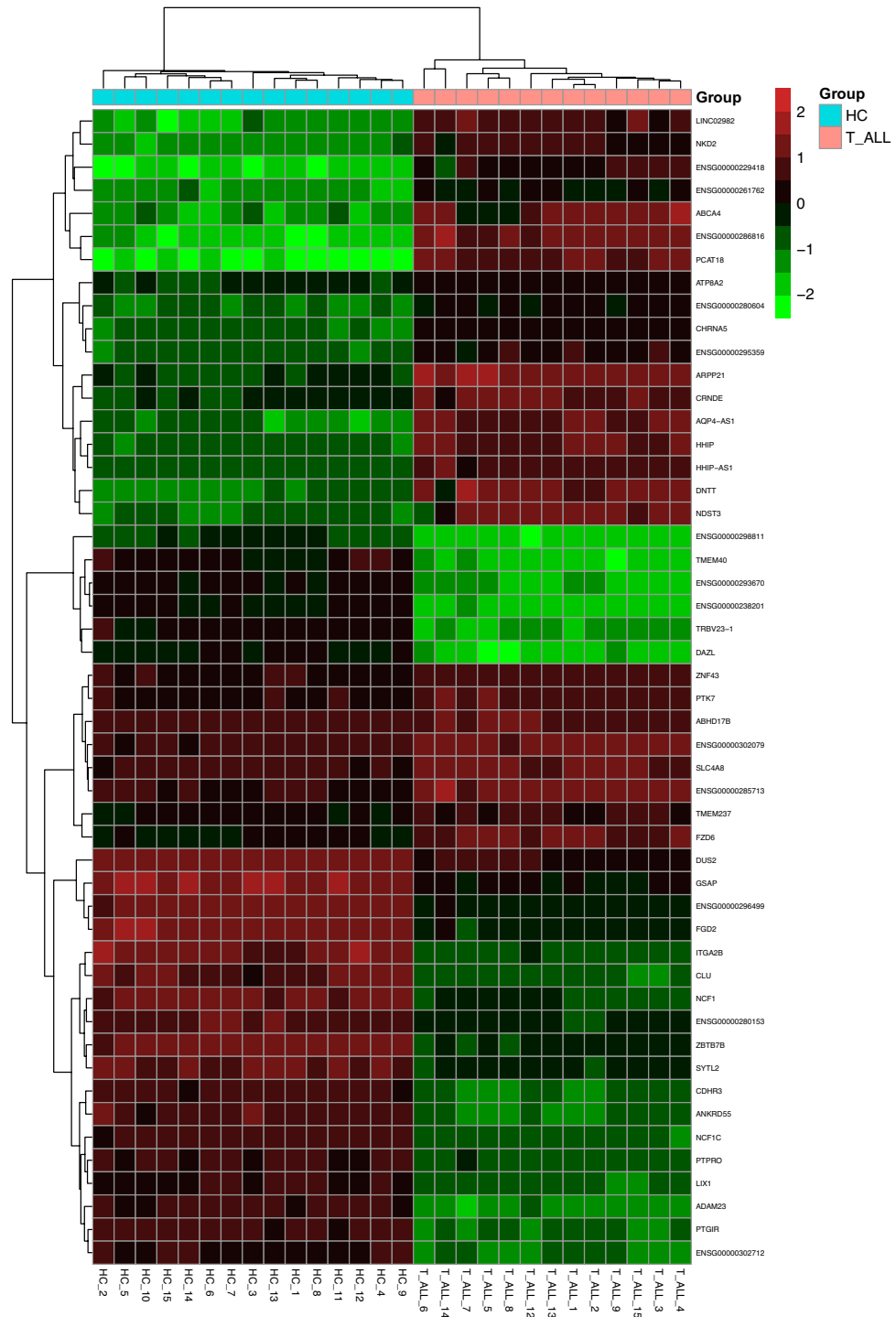


Fig. 1. Heatmap of differentially expressed genes. Heatmap representing \log_2 FoldChange of top 50 genes sorted by their significance (adjusted p-values). Upside plot shows the dendrogram derived from sample clustering while on rightside the clustering made on selected genes. Colorimetric scale reflect \log_2 FoldChange with under-expressed genes in green and over-expressed ones in red.

profiling of relevant cyclins indicated that while there was downregulation of Cyclins A, D and E there was relative upregulation of Cyclin B in PCAT18 silenced cells (Fig. 4F).

This relative dysregulation could represent an opportunity for a cell to progress to mitosis in a compensatory/dysregulated manner despite some degree of loss of function by disruption of the upstream checkpoint. The same experiments were conducted on a second human T-ALL cell line, RPMI8402, showing the same results (Supplementary Fig. 2). These findings lend supports the hypothesis that PCAT18 participates in the orderly regulation of cell cycle transitions in T-ALL.

A

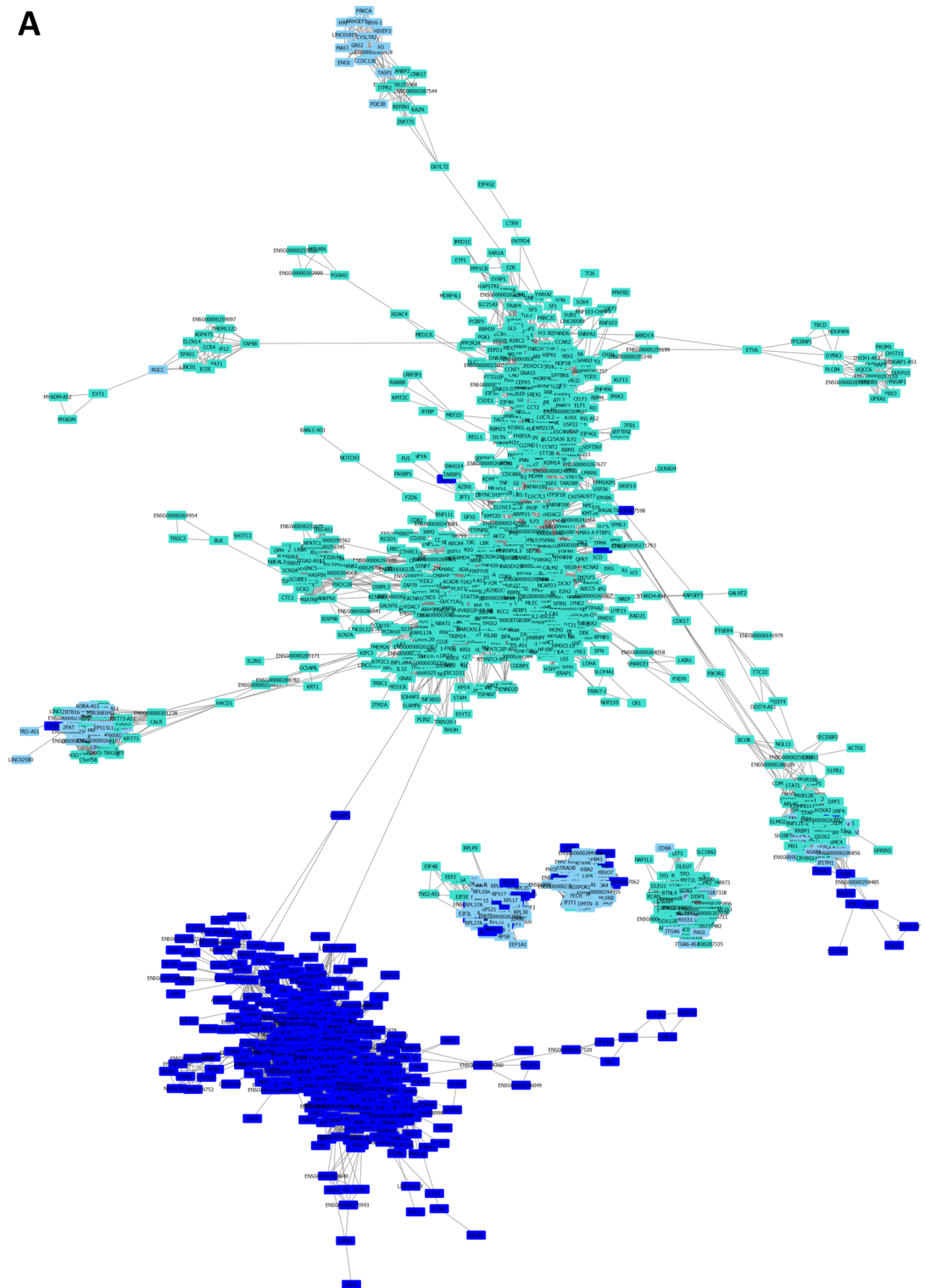


Fig. 2. Weighted gene co-expression network analysis (WGCNA) of the top 2,500 most variable genes. Gene co-modulation networks generated using weighted gene co-expression network analysis (WGCNA) on the top 5000 genes ranked by expression variance. The resulting network was imported into Cytoscape for visualization. **(A)** Network with nodes labeled by gene–module membership. **(B)** Network with nodes labeled by \log_2 FoldChange. **(C)** Correlogram showing correlations between study groups and the identified gene modules.

Transcriptomic profiling following PCAT18 silencing

To deeply investigate the molecular effects of PCAT18 deficiency in T-ALL, we performed RNA-seq on JURKAT cells silenced for this lncRNA and relative control using Illumina NovaSeq6000 technology. Differential

B

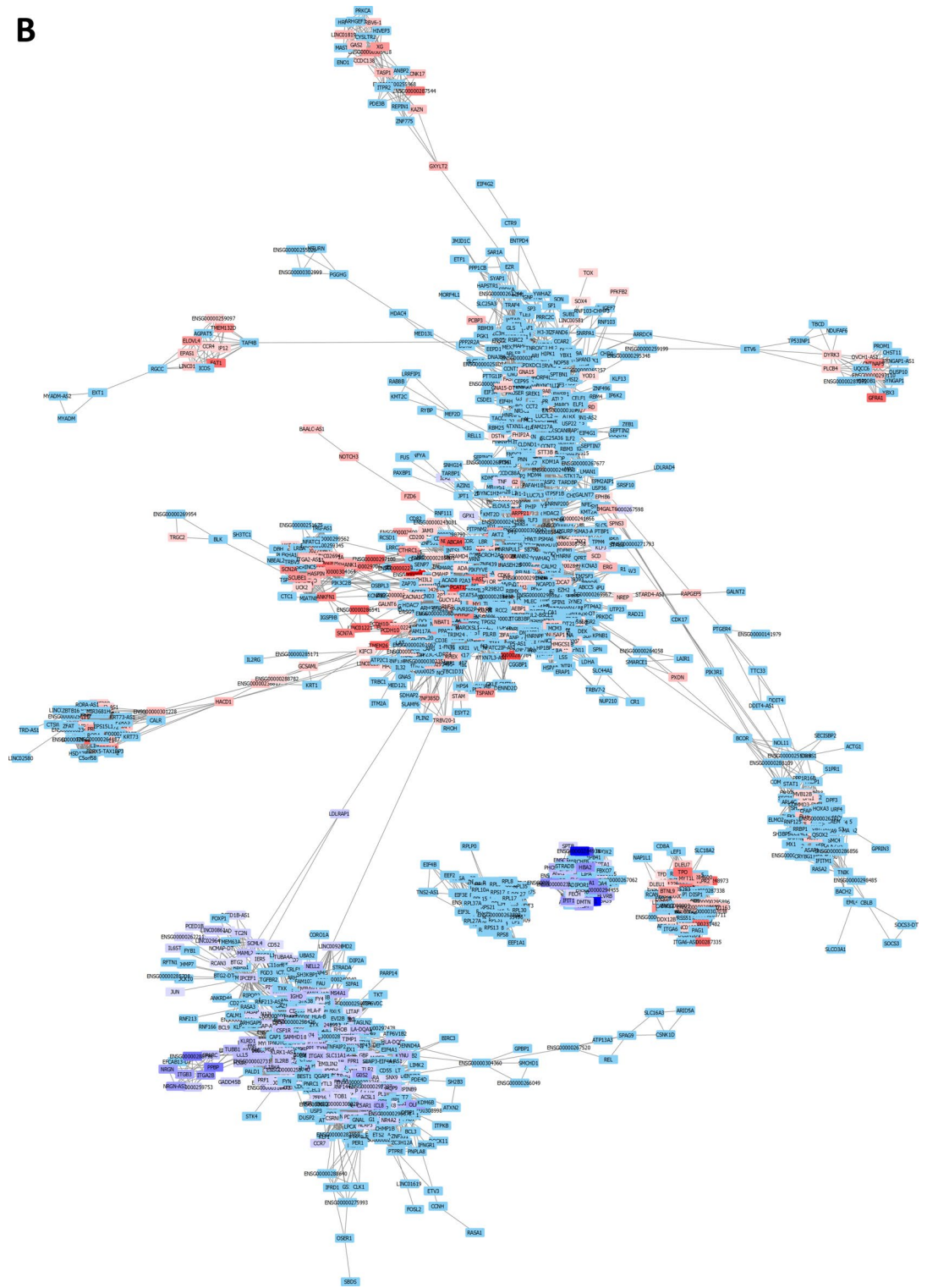


Fig. 2. (continued)

expression analysis using DESeq2 showed a huge transcriptional difference in silenced samples compared with control. A useful step in an RNA-Seq analysis is often the evaluation of the general similarity between the samples. To do this we performed the Euclidean distances among all samples in each condition considered. So, we performed the quality control check, such as PCA among all samples considered (Fig. 5A). Genes showing adjusted p -values ≤ 0.05 (padj), were considered as significant differentially expressed genes. Interestingly, several stress-response genes, such as HSP90AA1 and HSPA8, were found to be significantly up-regulated in the silenced condition, thus a compensatory mechanism triggered by proteotoxic or proliferative stress as a

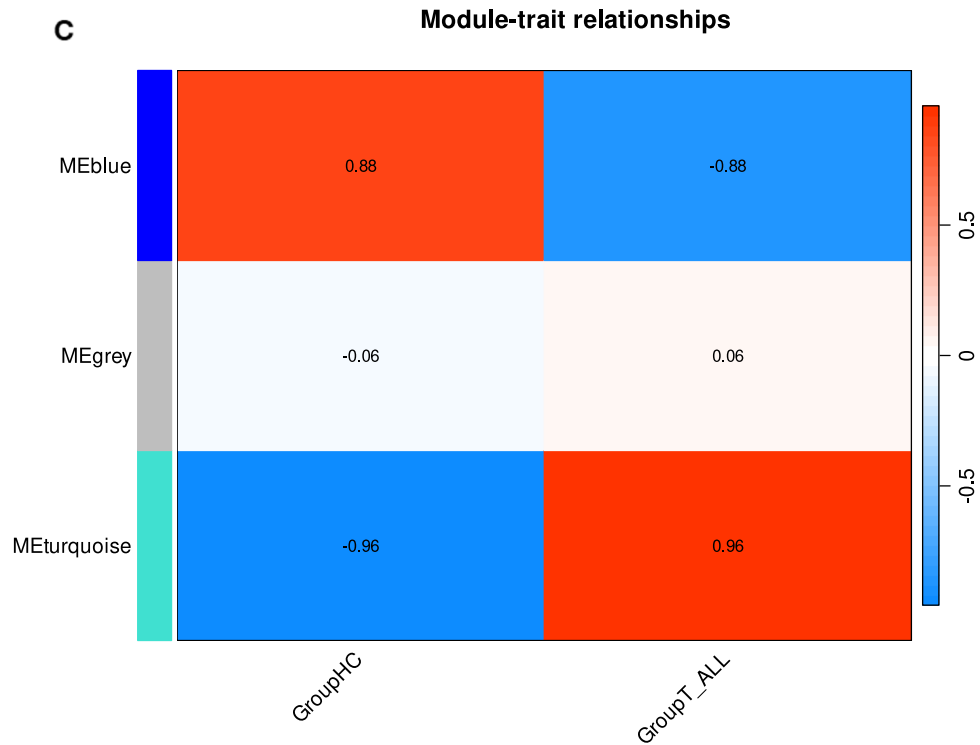


Fig. 2. (continued)

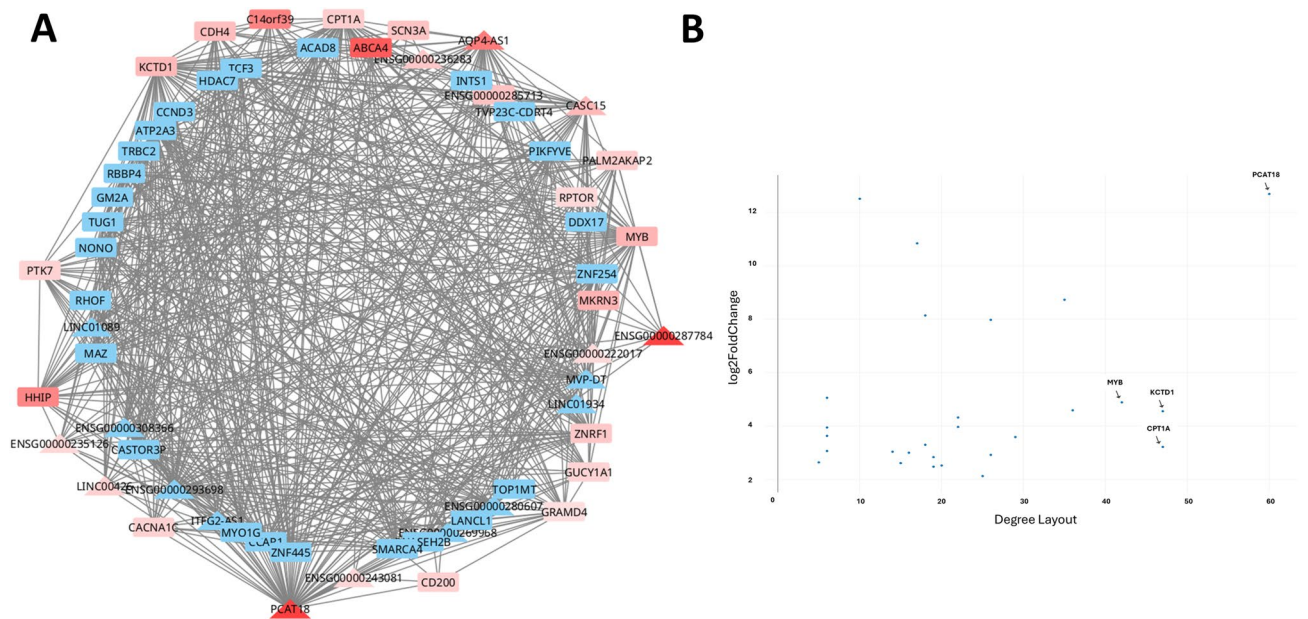


Fig. 3. Report genetic elements (coding and non-coding) predicted to be co-modulated with PCAT18. **(A)** Sub-network centered on PCAT18, obtained by extracting all connected nodes from the global network. Nodes are arranged in a circular layout, with colors representing log₂FoldChange values (red = upregulated, blue = downregulated). Node shapes distinguish coding genes (rounded squares) from non-coding elements (triangles), highlighting the functional diversity of PCAT18-associated interactions. **(B)** Scatterplot representing PCAT18 co-modulated elements plotted for their log₂FoldChange over Degree (the number of linked neighbors). On the top right are placed elements with highest connectivity and log₂FoldChange.

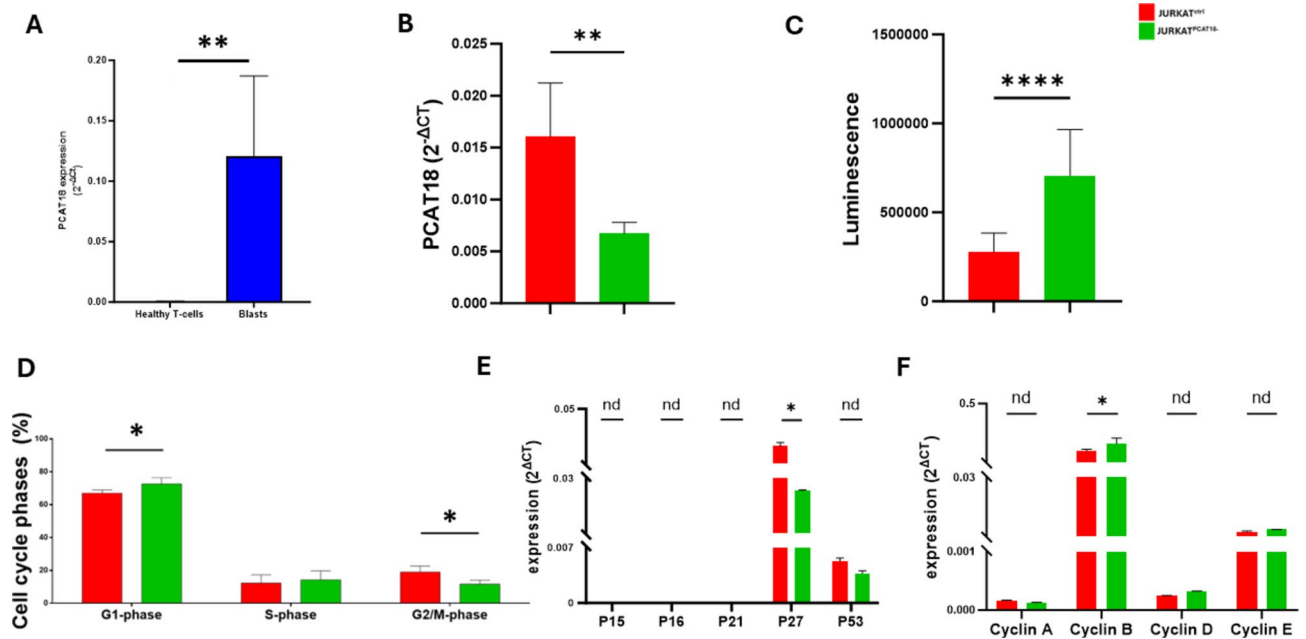


Fig. 4. Effect of PCAT18 silencing on T-ALL cell viability. **(A)** Quantitative RT-PCR analysis of PCAT18 expression in sorted cell populations from paediatric T-ALL samples in Blast cells (blue bar) and healthy T-cells (black bar). **(B)** PCAT18 expression level in JURKAT^{PCAT18-} cells (green bar) and JURKAT^{ctrl} cells (red bar) after 48 h of transfection. Expression levels are represented as $2^{-\Delta\text{Ct}}$ values. Data are mean \pm SD of three independent experiments. **(C)** Cell viability assay measured in JURKAT^{PCAT18-} cells (green bar) and JURKAT^{ctrl} cells (red bar) after 48 h of transfection using a luminescent ATP-based assay. **(D)** Flow cytometry analysis of cell cycle phases (G1, S, G2/M) JURKAT^{PCAT18-} cells (green bar) and JURKAT^{ctrl} cells (red bar) after 48 h of transfection. Data represent the mean percentage of cells in each phase \pm SD of three independent experiments. **(E)** qRT-PCR analysis of p15, p16, p21, p27 and p53 and of cyclins **(F)** in JURKAT^{PCAT18-} cells (green bar) and JURKAT^{ctrl} cells (red bar). Data are normalized to RPS18 and shown as mean \pm SD of three independent experiments. * = p-value < 0,05. nd = Not Determined. Mann-Whitney T-test.

result of PCAT18 loss was probably involved (Fig. 5B). In contrast, transcription factors and lineage-specific regulators like FOXP3 and NOTCH3 resulted downregulated, suggesting that PCAT18 could be a more general factor, regulating T-cell identity along with differentiation signals. Pathway enrichment analysis performed with the pathfinder package (KEGG database)²⁴ revealed again a number of biological processes that were affected by PCAT18 silencing (Fig. 5C). The enriched pathways concerned protein folding, chaperone-assisted assembly of protein complexes, and Notch signalling, thus indicating transcriptional changes. Visual inspection through plots such as bubble plots and term-gene heatmaps, confirmed the role of many genes toward various mutually interrelated pathways with HSP90AA1 as recurrent node in most of the functional clusters (Fig. 5C). These *in silico* results were validated through Real-Time PCR experiments, which confirmed the upregulation of HSP90AA1 and HSPA8 and the decreased expression levels of FOXP3 and NOTCH3 (Fig. 5D).

In combination, these transcriptomic data imply that PCAT18 acts as a regulator of cell survival and T-lineage programming transcription factors, and that the decrease of the expression of PCAT18 leads to a loss of that regulating balance which may be at the base of the abnormal proliferation revealed by functional assays.

Discussion

LncRNAs have emerged as critical regulators in various cancers, including pediatric T-cell acute lymphoblastic leukemia influencing gene expression at the transcriptional, post-transcriptional, and epigenetic levels, making them important players in leukemogenesis^{25,26}.

In pediatric T-ALL, dysregulated lncRNA expression has been linked to altered cell proliferation, apoptosis resistance, and treatment response. Specific lncRNAs such as MALAT1, LUNAR1, T-ALL-R-lncR1, and MEG3 have shown functional significance in disease progression^{27–30}.

LncRNAs also contribute to chemoresistance in T-ALL, affecting the efficacy of current therapeutic regimens. Their cell-type and disease-stage specificity make them promising biomarkers for diagnosis, prognosis, and treatment stratification^(31–34).

In our previous study, we found a unique signature of long non-coding RNAs that could differentiate between paediatric T-ALL and B-ALL cases¹⁰.

Our integrative transcriptomic analysis T-ALL and cord blood mononuclear cell controls revealed widespread gene expression reprogramming in which PCAT18 emerged as a central node within a disease-associated co-expression module, suggesting a potentially important regulatory role in T-ALL pathogenesis. PCAT18

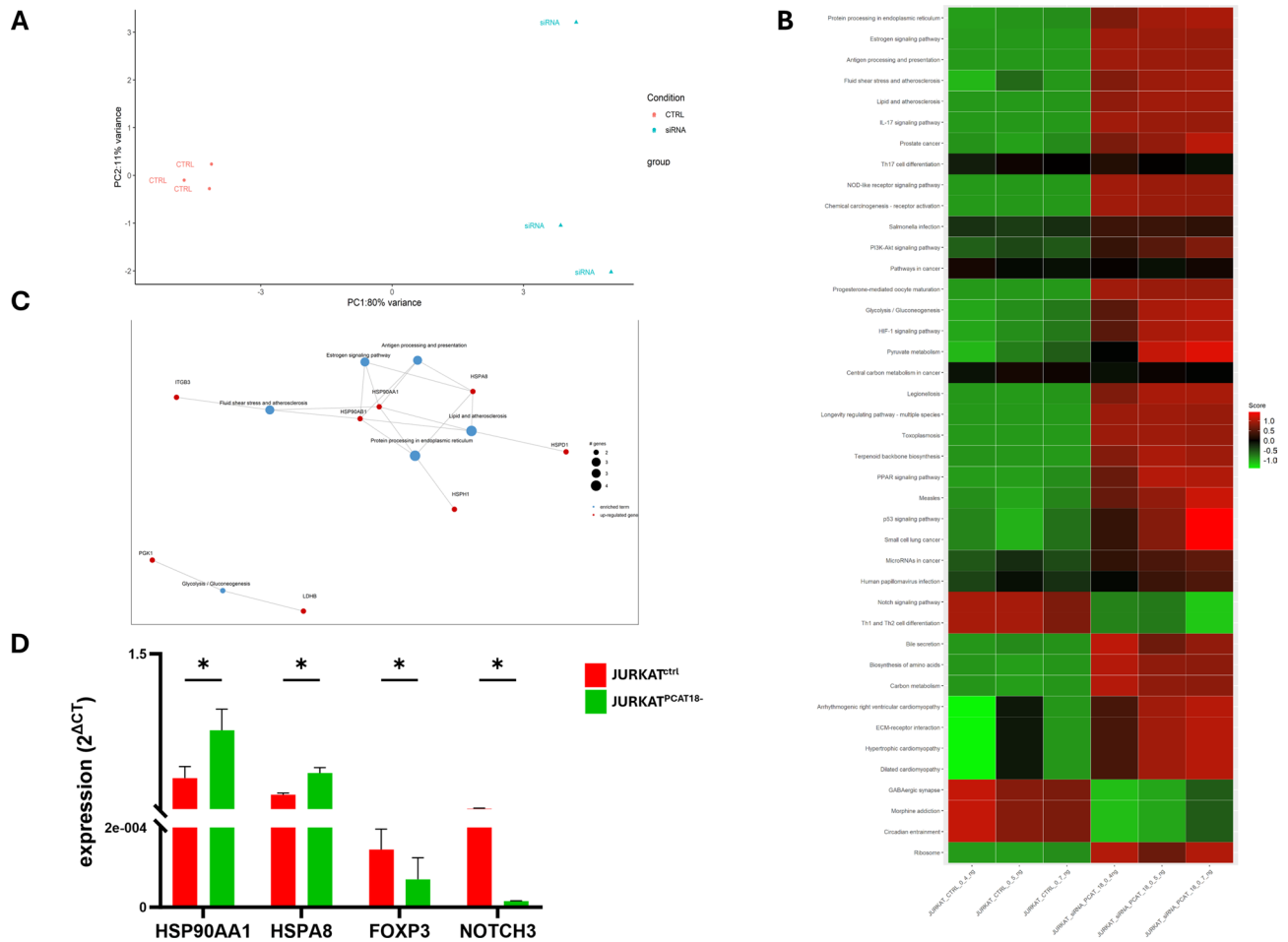


Fig. 5. RNA-seq analyses of PCAT18 silenced T-ALL cells. **(A)** Principal Component Analysis (PCA) plot based on the top differentially expressed genes clearly distinguishes JURKAT^{PCAT18-} cells (cyan triangles) from JURKAT^{ctrl} (red circles). **(B)** Upregulated genes in the JURKAT^{PCAT18-} (red nodes) include heat shock proteins such as HSP90AA1 and HSPA8, which cluster around multiple stress-related enriched pathways (blue nodes). **(C)** KEGG pathway analysis comparing JURKAT^{PCAT18-} and JURKAT^{ctrl} conditions shows upregulation (red) of stress- and chaperone-related pathways in JURKAT^{PCAT18-} cells, and relative downregulation (green) of immune-related and T-cell differentiation pathways. Color scale indicates enrichment score from -1 (downregulated) to +1 (upregulated). Pathway maps adapted from KEGG (Kyoto Encyclopedia of Genes and Genomes, www.kegg.jp): Protein processing in endoplasmic reticulum (hsa04141) and Notch signaling pathway (hsa04330). Copyright © Kanehisa Laboratories. Used with permission. **(D)** qRT-PCR validation of dysregulated HSP90AA1, HSPA8, FOXP3 and NOTCH3 genes in JURKAT^{PCAT18-} cells (green bar) and JURKAT^{ctrl} cells (red bar). Data are normalized to RPS18 and presented as mean ± SD from three independent experiments. * = p-value < 0,05. Mann–Whitney T-test.

has been previously described in the context of prostate and gastrointestinal cancers, where it is implicated in cell proliferation and epithelial–mesenchymal transition (EMT). However, its function in hematological malignancies has remained largely unexplored. WGCNA conducted on the top 2,500 most variable genes, identified a turquoise module strongly associated with the T-ALL phenotype (Spearman $r = 0.96$), within which PCAT18 was a highly connected node. The construction of a PCAT18-centered subnetwork comprising 61 co-expressed genes further supports its potential role as a regulatory hub in leukemia-specific transcriptional programs. Importantly, the PCAT18 subnetwork includes both protein-coding genes and other non-coding elements, indicating a complex interplay between regulatory RNA species and canonical signaling or metabolic pathways. The \log_2 FoldChange vs. node degree plot highlights several highly connected genes with extreme differential expression, which may serve as key effectors or co-regulators of PCAT18 function. The presence of numerous differentially expressed hub genes in proximity to PCAT18 strengthens the hypothesis that it may orchestrate or reflect broader transcriptional dysregulation in T-ALL.

The identification of a PCAT18-driven co-expression network is particularly noteworthy given the emerging recognition of lncRNAs as modulators of chromatin architecture, transcription factor activity, and RNA stability. In the context of T-ALL, where dysregulated transcriptional control is a hallmark of disease progression, PCAT18 may serve as a functional node linking non-coding transcription to oncogenic signaling networks. Furthermore,

the disease-specific nature of the PCAT18 network suggests that it may be leveraged as a biomarker for T-ALL stratification or as a candidate for therapeutic targeting, pending functional validation.

In our manuscript, we began to clarify the functional role of PCAT18 by investigating it in two cellular models of T-ALL, emphasizing its surprising role as a negative regulator of leukemia cell proliferation. Unlike its pro-oncogenic function in solid tumours, knocking-down PCAT18 in JURKAT cells produced a clear proliferative advantage and change in the cell cycle profile, specifically an accumulation in the G1 phase. The reduction of the cyclin-dependent kinase inhibitor p27 supports the finding of de-repressed checkpoint control at the G1/S transition.

Moreover, the selective increase of Cyclin B, a key regulator of the G2/M transition, indicates a compensatory change in how the cell regulates its cell cycle. Although the G1 phase arrest was dominant, the high levels of Cyclin B may indicate that cell is trying to overcome this block to try the transition into mitosis, in spite of a disparity upstream. Disruption of this regulation is characteristic of malignant proliferation and may suggest that the loss of PCAT18 not only disrupts checkpoint fidelity but also the sequencing of cell cycle transitions. At the same time, our data pose an intriguing biological paradox. PCAT18 is highly expressed in leukemic T-ALL blasts and is not detectable in normal T cells, a profile that normally would be indicative of an oncogenic role. Yet, its silencing led to increased proliferation in the two leukemic cell models tested. One possibility is that PCAT18 is ectopically activated in T-ALL as part of a leukemia-specific compensatory or feedback mechanism to restrain overproliferation. In this case, its expression could be seen as an adaptive transcriptional response to oncogenic stress rather than a transforming event. The absence of PCAT18 would then unleash proliferative constraints, thus facilitating unchecked cell cycle progression. This duality is in line with the evolving understanding that lncRNAs can act as oncogenes or tumor suppressors depending on their cellular and epigenetic environment. Further complementary approaches, including PCAT18 overexpression, will be necessary to fully clarify the biological role of PCAT18 in T-ALL. Knock-down of PCAT18 forced upregulation of both HSP90AA1 and HSPA8 that suggest activation of stress response pathways likely related to either proteome instability due to increased metabolic demand in a deregulated proliferative phenotype. At the same time, the downregulation of FOXP3 and NOTCH3 suggests collateral breakdown of both immune regulatory networks and lineage fidelity, both essential components of T-cell identity during haematopoiesis and transformation.

While our study provides the first functional characterization of PCAT18 in pediatric T-ALL, we recognize several limitations that must be considered when interpreting these findings. Primarily, our functional assays were conducted using *in vitro* models (JURKAT and RPMI8402 cell lines), which, although established in leukemia research, may not fully replicate the complex bone marrow microenvironment or the systemic interactions present *in vivo*. Consequently, while the paradoxical increase in proliferation alongside G1 accumulation and Cyclin B upregulation suggests a disruption of cell cycle fidelity, further validation in *in vivo* models or patient-derived xenografts (PDX) is necessary to confirm these regulatory mechanisms and the proposed tumor-suppressive role. Furthermore, while the WGCNA successfully identified PCAT18 as a high-connectivity node within a T-ALL-specific module, it is important to note that these co-expression patterns signify correlations and do not definitively establish causation. Although we addressed this by performing transcriptomic profiling of PCAT18-silenced cells, the subnetwork extraction and hub-gene identification remain dependent on the statistical thresholds applied. Finally, despite the high lineage specificity of PCAT18 expression across our patient cohort, the limited size and clinical heterogeneity of the study population precluded a comprehensive analysis of the correlation between PCAT18 levels and long-term clinical outcomes, such as relapse or overall survival. Longitudinal studies involving larger, multicenter cohorts are required to robustly define PCAT18's utility as a diagnostic or prognostic biomarker.

Despite this our findings could reinforce the hypothesis that PCAT18 acts at the intersection of cell cycle regulation, transcriptional control and stress adaptation in T-ALL. The overall imbalance amongst cyclins, particularly with regard to Cyclin B overexpression, could represent a readout of uncoordinated cell cycle progression in the absence of PCAT18 and reinforced the potential of PCAT18 to selectively modulate late-stage cell cycle regulators.

Conclusions

Collectively, these findings indicate that PCAT18 is not merely a passive transcript but may act as a lineage- and stage-specific tumor suppressor-like regulator and potential clinical biomarker in T-ALL, particularly where its loss contributes to dysregulation of proliferation, stress responses, and T-cell transcriptional programs. Our data suggest that, in contrast to its established pro-oncogenic role in solid tumours, PCAT18 exhibits distinctly different context-dependent behavior in the setting of T-ALL.

These insights not only expand our understanding of lncRNAs biology in leukemia but also open new avenues for the development of diagnostic and potentially therapeutic strategies targeting non-coding RNA networks in paediatric T-cell leukemia.

Data availability

Raw sequencing reads were loaded to NCBI bioproject number PRJNA1263624. Contact corresponding authors F.A. (Filomena.altieri@synlab.it) for other information.

Received: 7 November 2025; Accepted: 28 March 2026

Published online: 03 April 2026

References

- Pui, C. H. et al. Childhood Acute Lymphoblastic Leukemia: Progress Through Collaboration. *J Clin Oncol.* **33**(27), 2938–2948 (2015).
- Inaba, H. & Mullighan, C. G. Pediatric acute lymphoblastic leukemia. *Haematologica* **105**(11), 2524–2539 (2020).
- Pui, C. H., Carroll, W. L., Meshinchi, S. & Arceci, R. J. Biology, risk stratification, and therapy of pediatric acute leukemias: an update. *J Clin Oncol Off J Am Soc Clin Oncol.* **29**(5), 551–565 (2011).
- Guttman, M. & Rinn, J. L. Modular regulatory principles of large non-coding RNAs. *Nature* **482**(7385), 339–346 (2012).
- Zhang, H. et al. Long non-coding RNA: a new player in cancer. *J Hematol Oncol Hematol Oncol.* **31**(6), 37 (2013).
- Batista, P. J. & Chang, H. Y. Long noncoding RNAs: cellular address codes in development and disease. *Cell* **152**(6), 1298–1307 (2013).
- Esteller, M. Non-coding RNAs in human disease. *Nat Rev Genet.* **12**(12), 861–874 (2011).
- Filomena, A. et al. Identification of a circular RNA isoform of WASHC2A as a prognostic factor for high-risk paediatric B-ALL patients. *Biomed Pharmacother Biomedicine Pharmacother.* **177**, 116903 (2024).
- Altieri, F. et al. LINC00958 as new diagnostic and prognostic biomarker of childhood acute lymphoblastic leukaemia of B cells. *Front Oncol* <https://doi.org/10.3389/fonc.2024.1388154> (2024).
- Buono, L. et al. Specific lincRNA signatures discriminate childhood acute leukaemias: a pilot study. *Cancer Cell Int.* **22**(1), 373 (2022).
- Prensner, J. R. et al. Transcriptome sequencing across a prostate cancer cohort identifies PCAT-1, an unannotated lincRNA implicated in disease progression. *Nat. Biotechnol.* **29**(8), 742–749 (2011).
- Chen, P. et al. The Down-Regulation of lincRNA PCAT18 Promotes the Progression of Gastric Cancer via MiR-107/PTEN/PI3K/AKT Signaling Pathway. *OncoTargets Ther.* **13**(12), 11017–11031 (2019).
- Mirabelli, P. et al. SDN Biobank: Biosource of Human Samples Associated with Functional and/or Morphological Bioimaging Results for the Study of Oncological, Cardiological, Neurological, and Metabolic Diseases. *Open J Bioresour.* **4**(1), 2 (2017).
- Chen, S., Zhou, Y., Chen, Y. & Gu, J. fastp: an ultra-fast all-in-one FASTQ preprocessor. *Bioinforma Oxf Engl.* **34**(17), i884–i890 (2018).
- Dobin, A. et al. STAR: ultrafast universal RNA-seq aligner. *Bioinformatics* **29**(1), 15–21 (2013).
- Li, H. et al. The Sequence Alignment/Map format and SAMtools. *Bioinforma Oxf Engl.* **25**(16), 2078–2079 (2009).
- Liao, Y., Smyth, G. K. & Shi, W. featureCounts: an efficient general purpose program for assigning sequence reads to genomic features. *Bioinforma Oxf Engl.* **30**(7), 923–930 (2014).
- Liao, Y., Smyth, G. K. & Shi, W. The R package Rsubread is easier, faster, cheaper and better for alignment and quantification of RNA sequencing reads. *Nucleic Acids Res.* **47**(8), e47 (2019).
- Love, M. I., Huber, W. & Anders, S. Moderated estimation of fold change and dispersion for RNA-seq data with DESeq2. *Genome Biol.* **15**(12), 550 (2014).
- Langfelder, P. & Horvath, S. WGCNA: an R package for weighted correlation network analysis. *BMC Bioinform.* **29**(9), 559 (2008).
- Shannon, P. et al. Cytoscape: A software environment for integrated models of biomolecular interaction networks. *Genome Res.* **13**(11), 2498–2504 (2003).
- Zhu, L. et al. EZH2-mediated epigenetic suppression of lincRNA PCAT18 predicts a poor prognosis and regulates the expression of p16 by interacting with miR-570a-3p in gastric cancer. *J. Cancer.* **12**(23), 7069–7078 (2021).
- Cruz-Miranda, G. M. et al. Long non-coding RNA and acute leukemia. *Int. J. Mol. Sci.* **20**(3), 735 (2019).
- Farajzadeh, M. et al. Long noncoding RNAs in acute myeloid leukemia: biomarkers, prognostic indicators, and treatment potential. *Cancer Cell Int.* **5**(25), 131 (2025).
- Amodio, N. et al. MALAT1: a druggable long non-coding RNA for targeted anti-cancer approaches. *J. Hematol. Oncol. J. Hematol. Oncol.* **11**(1), 63 (2018).
- El-Khazragy, N. et al. Upregulation of leukemia-induced non-coding activator RNA (LUNAR1) predicts poor outcome in pediatric T-acute lymphoblastic leukemia. *Immunobiology* **226**(6), 152149 (2021).
- Zhang, L., Xu, H. G. & Lu, C. A novel long non-coding RNA T-ALL-R-LncR1 knockdown and Par-4 cooperate to induce cellular apoptosis in T-cell acute lymphoblastic leukemia cells. *Leuk. Lymphoma.* **55**(6), 1373–1382 (2014).
- Pei, J. S. et al. Novel Contribution of Long Non-coding RNA MEG3 Genotype to Prediction of Childhood Leukemia Risk. *Cancer Genomics Proteomics.* **19**(1), 27–34 (2022).
- Qu, Y. et al. The functional role of long noncoding RNA in resistance to anticancer treatment. *Ther. Adv. Med. Oncol.* **1**(12), 1758835920927850 (2020).
- Ghahramani Almanghadim H, Karimi B, porsalehi N, Sanavandi M, Atefi pourfardian S, Ghaedi K. The biological role of lincRNAs in the acute lymphocytic leukemia: An updated review. *Gene.* 2024 Mar 10;898:148074.
- Bhat, A. A. et al. Role of non-coding RNA networks in leukemia progression, metastasis and drug resistance. *Mol Cancer.* **19**(1), 57 (2020).
- Shi, H., Gao, L., Zhang, W. & Jiang, M. Long non-coding RNAs regulate treatment outcome in leukemia: What have we learnt recently?. *Cancer Med.* **12**(13), 13966–13977 (2023).

Author contributions

F.A., G.P., and V.C. designed and performed the experiments and data analyses and wrote the manuscript; G.B., R.P., G.Ben. and R.Par. diagnosed and treated the patients enrolled in this study; GS designed and performed the experiments and data analyses, wrote the manuscript and gave final approval. All authors have read and agreed to the published version of the manuscript.

Funding

This work was funded by the Italian Ministry of Health, partly (Ricerca Finalizzata—Giovani Ricercatori Under40) with Grant code GR-2021–12372945 entitled “Long non-coding RNAs and their role on epigenome as diagnostic markers in childhood acute lymphoblastic leukemia of T cells”, and partly, by “Progetti di Ricerca Corrente”.

Declarations

Competing interests

The authors declare no competing interests.

Ethics approval and consent to participate

The procedures followed in this study, in line with the Helsinki declaration, have been approved by the local

ethical committees of Naples- Italy (protocol number 5/19 of the 19 June 2019) and 1/23 (dated 8 February 2023) as well as the AORN Santobono-Pausilipon Cardarelli/Pausilipon Ethical Committee (Naples, Italy, protocol number 07/20 of 3 June 2020). Both parents signed informed consent.

Additional information

Supplementary Information The online version contains supplementary material available at <https://doi.org/10.1038/s41598-026-46929-5>.

Correspondence and requests for materials should be addressed to F.A.

Reprints and permissions information is available at www.nature.com/reprints.

Publisher's note Springer Nature remains neutral with regard to jurisdictional claims in published maps and institutional affiliations.

Open Access This article is licensed under a Creative Commons Attribution-NonCommercial-NoDerivatives 4.0 International License, which permits any non-commercial use, sharing, distribution and reproduction in any medium or format, as long as you give appropriate credit to the original author(s) and the source, provide a link to the Creative Commons licence, and indicate if you modified the licensed material. You do not have permission under this licence to share adapted material derived from this article or parts of it. The images or other third party material in this article are included in the article's Creative Commons licence, unless indicated otherwise in a credit line to the material. If material is not included in the article's Creative Commons licence and your intended use is not permitted by statutory regulation or exceeds the permitted use, you will need to obtain permission directly from the copyright holder. To view a copy of this licence, visit <http://creativecommons.org/licenses/by-nc-nd/4.0/>.

© The Author(s) 2026